Supporting information

Elongated magnetic nanoparticles with high-aspect ratio: a nuclear relaxation and specific absorption rate investigation

Matteo Avolio,[a] Helena Gavilán,[b] Eva Mazario,[b] Francesca Brero,[a] Paolo Arosio,[c] Alessandro Lascialfari,[c] M. Puerto Morales[b]

[a] Dipartimento di Fisica, INFN and INSTM, Università degli Studi di Pavia, Via Bassi 6, 27100, Pavia, Italy

[b] Departamento de Energía, Mediambiente y Salud, Instituto de Ciencia de Materiales de Madrid, ICMM/CSIC, Cantoblanco, 28049 Madrid, Spain

[c] Dipartimento di Fisica, INFN and INSTM, Università degli Studi di Milano, Via Celoria 16, 20133 Milano, Italy

SYNTHESIS OF ELONGATED PRECURSORS

Synthesis of Goethite elongated nanoparticles (e-MNPs)

For the goethite precursor synthesis (step (i)), solutions of Na_2CO_3 0.9 M and Fe(II)SO_4 0.075 M are prepared using distilled water in an inert atmosphere (achieved by bubbling N_2, in order to avoid Fe(II) oxidation). The molar ratio CO_3^-/Fe(II) = 12 is identified as the best choice for obtaining particles about 100 nm long. The Na_2CO_3 solution is prepared in a glass reaction vessel that allows to bubble nitrogen inside, while the temperature is kept at 40°C thanks to a thermal bath. Subsequently, the $FeSO_4$ is poured into the vessel. N_2 bubbling and a moderate magnetic stirring allow a homogeneous solution. The N_2 flux is then replaced overnight by a 2 L/min air flow to form goethite by aerial oxidation. Briefly, Fe(II) cations oxidize on aeration forming a solid phase of a mixture of sulphate and carbonate green-rusts, which decompose as a result of a further oxidation producing goethite. The obtained goethite nanoparticles suspension is centrifuged for 10 minutes at 7500 rpm, and the precipitate is washed several times with distilled water and lyophilized.

Silica coating of elongated nanoparticles

Particles are coated with silica (step (ii)) by applying the Stöber method[1,2]. For the successful coating of the elongated nanoparticles, we optimized the protocol as follows: in a 400 mL glass bottle, 100 mg of nanoparticles are added to 200 mL of 2-propanol and 100 mL of distilled water, and sonicated for 15 mins. Then, 20 mL of NH_4OH 28.0-20.0% V/V are added to the solution and mixed using ultrasounds for 5 mins. Finally, 200 µl of tetraethyl orthosilicate (TEOS) are added during sonication and the reaction is allowed to continue for 15 mins. The obtained sample is centrifuged for 45 minutes at 7500 rpm, washed with ethanol several times and then lyophilized.

STRUCTURAL CHARACTERIZATION OF THE ELONGATED NANOPARTICLES

Goethite crystal structure of the elongated nanoparticles was confirmed by both XRD and IR (Fig. S1) analysis, showing Bragg peaks at 2θ angles and wave numbers typical of goethite[3].

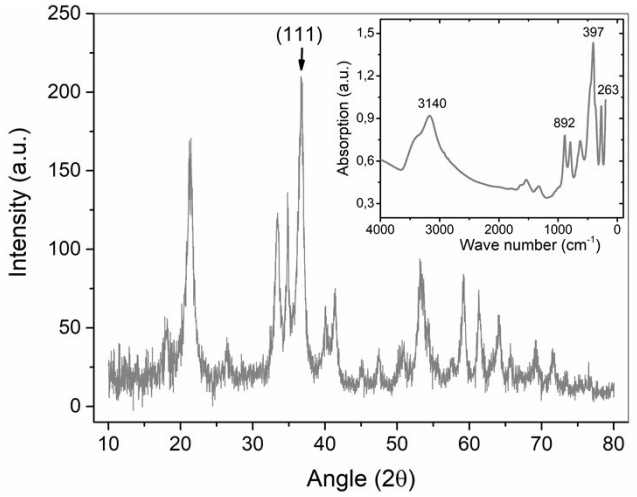

Figure S1. XRD pattern and IR absorption spectrum (inset) of the goethite precursor nanoparticles.

The goethite crystal dimensions obtained by fitting the (111) peak of the XRD pattern with the Scherrer equation resulted to be 9.9 ± 1.5 nm; considering that the major axis of the e-MNPs lies along the [100] axis of goethite, particles result to be polycrystalline or characterized by an amorphous structure for most of their volume.

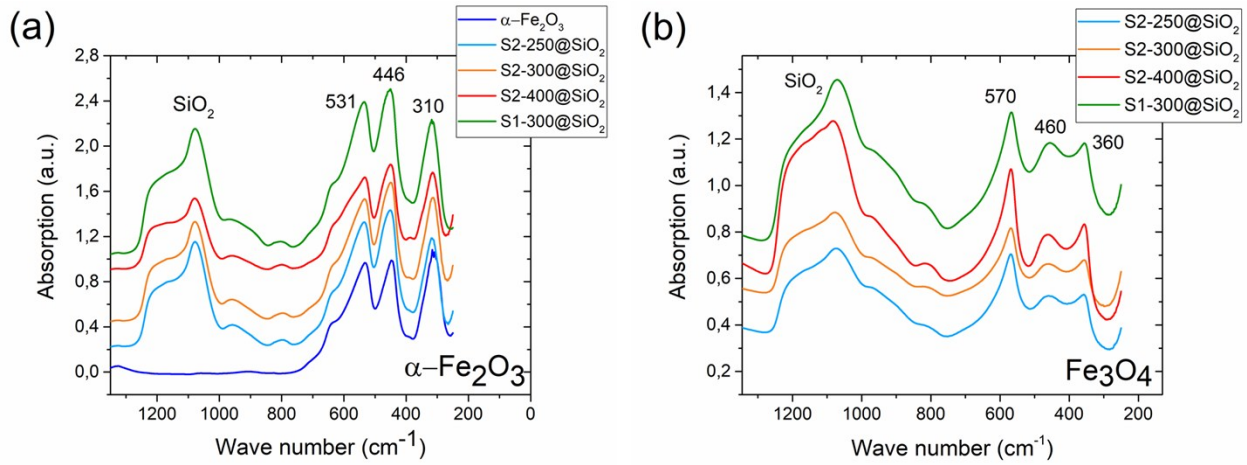

Figure S2. IR absorption spectra of (a) the four hematite precursors coated with silica, compared to the spectrum of a pure hematite sample to evince the presence of the silica coating; (b) the four samples totally reduced to magnetite.

After (step (ii)) of the synthesis, the presence of the silica coating was successfully verified by IR spectroscopy (Fig. S2). In fact, in each spectrum a large peak at wave numbers from 1250 to 1000 cm^{-1} is clearly detectable, a fingerprint of the silica molecules vibrations as described in Ref. 4.

Crystal size analysis was performed on the hematite precursors obtained after the dehydration process (step(iii)). Considering that the major axis of the e-MNPs is oriented along the [010] axis of hematite, the crystallinity value of α-Fe_2O_3 as seen by the XRD spectrum analysis (Table S1) is compatible with a monocrystalline structure.

Similarly, after the complete transformation of hematite into magnetite, the characteristic (311) peak of magnetite in the XRD spectrum was used to evaluate the crystallinity of the particles (Table S1), whose major axis is aligned along the [100] axis of magnetite. From the values reported in Table S1, it is interesting to observe that samples heated at increasing temperatures present increasing values of the crystal size. This behaviour could be related to the different porosity of the samples.

Table S1. Crystal size of the hematite precursor and of the magnetite samples as obtained from the XRD pattern analysis[a].

Sample	α-Fe_2O_3 (110) (nm)	Fe_3O_4 (311) (nm)
S2-250	19.0 ± 2.9	8.9 ± 1.4
S2-300	18.3 ± 2.8	10.4 ± 1.6
S2-400	21.1 ± 3.2	15.0 ± 2.3
S1-300	/[b]	10.5 ± 1.6

[a]Analysis was performed by fitting the (110) peak of hematite and the (311) peak of magnetite.

[b]In the strategy 1 (S1) the hematite elongated nanoparticles are already coated with silica, whose signal dominates the XRD pattern.

FURTHER INFORMATION ABOUT THE COLLOIDAL PROPERTIES OF THE SAMPLES

To deepen the analysis of the hydrodynamic size observed by means of DLS, the dimensions obtained examining either the intensity, volume or number peaks of the scattered light are reported in Table S2. The intensity peak, also reported in Table 1, is the only estimation of the e-MNPs size directly obtained from the scattered light, and it is typically considered the most reliable one. The spectrum is in fact given by a series of peaks corresponding to particles with different sizes and with intensity proportional to the amount of light scattered from each particle, which is approximately proportional to the sixth power of its diameter. The volume peak is an estimation of the size obtained by rearranging the intensity data, assuming spherical particles with

homogeneous and known optical properties (i.e. refractive index). In this case, the spectrum is made by peaks whose intensity is proportional to the volume of the particles. Finally, the number peak is an estimation obtained from the volume peak through a further data processing, that leads to a spectrum whose peaks intensity is proportional to the number of particles with a given size inside the sample[5]. As it can be easily understood, the volume and number peaks are highly susceptible to errors, which propagates from the light intensity distribution. Consequently, they are rarely utilized, and only the intensity peak is generally reported. However, samples whit high stability should give similar results for the three values of the hydrodynamic size. Hence, they are all reported in Table S2, and they result to be most of the times in excellent agreement among them, excluding the presence of aggregates within the samples.

Table S2. Hydrodynamic size (number, volume and intensity peaks – details are given in the text) of the magnetite e-MNPs, coated with both silica and dextran, as obtained from DLS analysis.

Sample	Number peak (nm)	Volume peak (nm)	Intensity peak (L_{DLS}) (nm)
S2-250	115 ± 7	118 ± 7	118 ± 4
S2-300	118 ± 7	122 ± 8	122 ± 6
S2-400	154 ± 10	159 ± 10	156 ± 7
S1-300	89 ± 17	97 ± 21	101 ± 17

HYPERTHERMIA MEASUREMENTS

Exemplary heating curves acquired on the sample S2-400 at f = 109.8 kHz and different field amplitudes are reported in Figure S3. The initial-slope method results to be correctly applicable to those curves due to the perfect linear trend observed up to 40 seconds heating. However, for longer times dissipation effects and particles instability (measurements were performed on e-MNPs coated only with silica) could determine a wrong estimation of the SAR due to the decrease of the $T(t)$ curve slope. For these reasons, the fits to determine $\Delta T/\Delta t$ were performed in the time intervals from 5 to 20 seconds after the switching on of the field (occurring at about t = 5 s in Fig. S3).

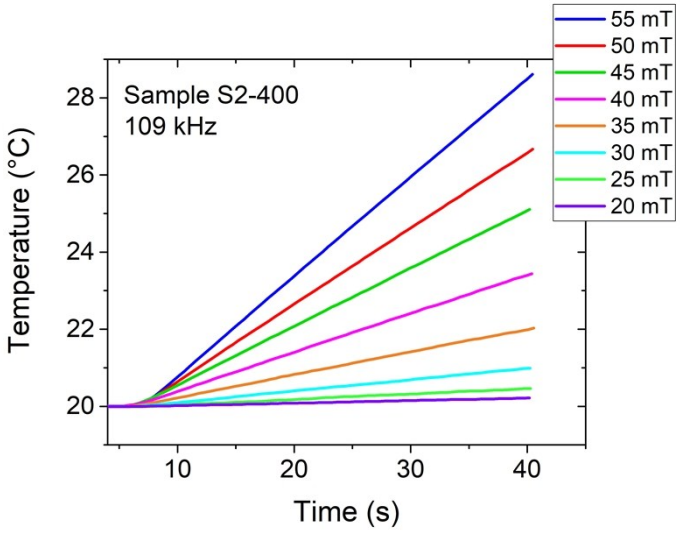

Figure S3. Heating curves acquired on the Sample S2-400 at f = 109.8 kHz and different field ampitudes.

PARTIALLY REDUCED SAMPLES

Synthesis

If the reduction (step (iv) of the synthesis) is stopped after the first 30 minutes, not all the hematite is allowed to transform to magnetite, leading to a mixed composition of magnetite and hematite in the e-MNPs cores. Three partially reduced samples were prepared, starting from the same hematite precursors used for the totally reduced samples (i.e. the magnetite samples presented in the main text). These samples are named as S2-250-P, S2-300-P and S2-400-P, with a "P" marking the partial reduction.

Morphological characterization of the samples

Statistical analysis of the TEM pictures acquired after the partial reduction of hematite to magnetite did not evidence appreciable changes in the particles size, which remain equal to those of the hematite precursors reported in Table 1.

XRD analysis (Fig. S4a) confirmed the presence of both iron oxide phases since characteristic peaks of both hematite and magnetite were identified in the diffraction pattern. XRD analysis was performed on peaks exclusive of hematite or maghemite; particularly, the (311) peak of magnetite is superimposed to the (110) peak of hematite and cannot be used for this analysis. Similarly, all the overlapping peaks were discarded. Table S3 shows the crystal size of both hematite and magnetite as obtained considering the exclusive peaks of magnetite ((400), (220)) and hematite ((104), (103)). As for the totally reduced samples, an increasing crystal size with increasing dehydration temperature was observed in the partially reduced samples, and the sample S2-400-P

turned out to be the one with the largest crystals. Interestingly, hematite crystals resulted to be larger in the (113) plane compared to the (104) plane only for the sample S2-250-P, while the two other samples showed comparable crystals size in the two planes. Regarding magnetite, the crystal size is larger in the plane (220) compared to the plane (400) for the samples S2-250-P and, particularly, for the sample S2-400-P, while no consistent differences are observed for the sample S2-300-P.

Similarly to the XRD patterns, also the IR spectra (Fig. S4b) resulted to be a convolution of the characteristic absorption peaks of pure hematite and magnetite.

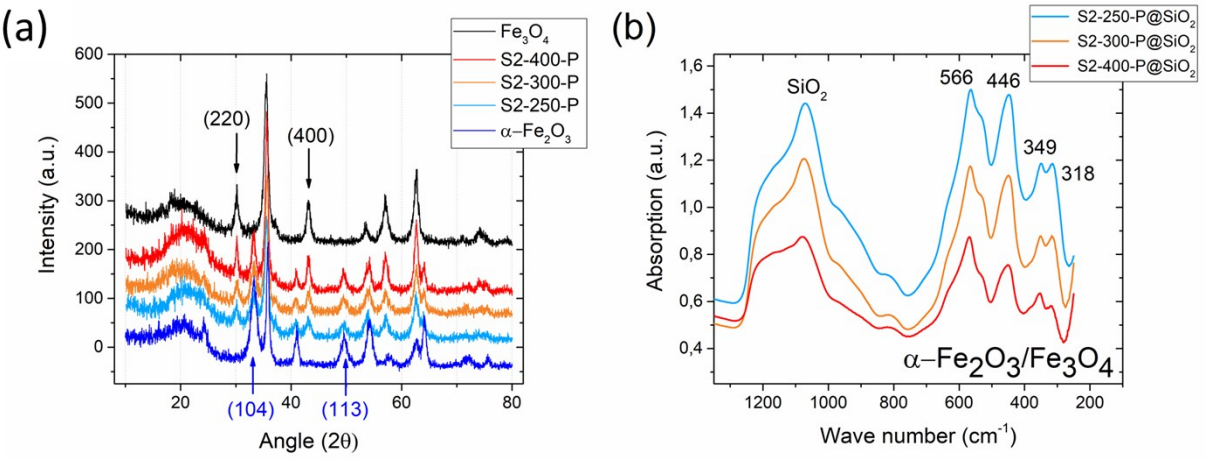

Figure S4. XRD patterns of the three samples partially reduced to magnetite, compared to the patterns of pure magnetite (black line) and hematite (blu line). Bragg Peaks used for the crystal size analysis, by means of Scherrer equation, are highlighted by black arrows for magnetite and blu arrows for hematite. (b) IR absorption spectra of the three samples partially reduced to magnetite: a convolution of the characteristic absorption peaks of pure magnetite and hematite is observed, attesting a mixed composition of those samples.

Table S3. Crystal size of hematite and magnetite within the partially reduced samples as obtained from the XRD pattern analysis. Analysis was performed by fitting the (104) and (113) peaks of hematite and the (400) and (220) peaks of magnetite.

Sample	α-Fe_2O_3 (104) (nm)	α-Fe_2O_3 (113) (nm)	Fe_3O_4 (400) (nm)	Fe_3O_4 (220) (nm)
S2-250-P	5.8 ± 0.9	8.3 ± 1.3	9.7 ± 1.5	13.0 ± 2.0
S2-300-P	7.4 ± 1.1	7.8 ± 1.2	12.3 ± 1.9	12.1 ± 1.8
S2-400-P	12.1 ± 1.8	11.8 ± 1.8	14.6 ± 2.2	24.9 ± 3.8

The porosity of the partially reduced samples was measured with the BET method only for the sample S2-300-P (Table S4): since it resulted to be compatible with that of the corresponding totally reduced sample S2-300 (Table 2), we concluded that no differences in porosity are induced by different reduction times.

Table S4. Specific Surface Area evaluated with the BET method for the samples S2-300-P and S2-300 (from Table 2). Both adsorption and desorption data of N_2 are reported.

Sample	Adsorption (m^2/g)	Desorption (m^2/g)
S2-300-P	69.1 ± 6.9	68.2 ± 6.8
S2-300	76.3 ± 7.6	72.3 ± 7.2

It is worth nothing that for the partially reduced samples, further analyses would be necessary to accurately describe the composition of the final samples. Hydrogen could activate the reduction process that converts hematite to magnetite both on the outer and inner (pores) surface of the particles, therefore it is not straightforward to describe the distribution of the two iron oxides within the particle volume. The partially reduced samples may consist of small magnetite clusters embedded in a hematite matrix, with magnetic properties perhaps more similar to those of superparamagnets and therefore more suitable to heat efficiently under the action of the AMFs typical of MFH, compared to the totally reduced ones.

Characterization of the colloidal properties of the samples

As for the totally reduced samples, negative values of the Z-potential (≈ -26 mV) confirmed the stabilization of the samples via electrostatic repulsion. A good colloidal stability of the samples was also confirmed by DLS measurements reported in Table S5, which excluded the presence of aggregates.

Table S5. Hydrodynamic size (number, volume and intensity peaks) of the e-MNPs partially reduced to magnetite, coated with both silica and dextran, as obtained from DLS analysis.

Sample	Number peak (nm)	Volume peak (nm)	Intensity peak (L_{DLS}) (nm)
S2-250-P	96 ± 19	105 ± 23	110 ± 20
S2-300-P	124 ± 21	131 ± 23	131 ± 17
S2-400-P	119 ± 17	122 ± 17	122 ± 12

Magnetic characterization of the samples

The hysteresis loops of the samples at T = 290 K and T = 5 K are reported respectively in Fig. S5a and Fig. S5b. Values of the saturation magnetization M_S as obtained from the fits of the loops at high fields with the Langevin function and of the coercive field H_C (insets of Fig. S5) are reported in Table S6. As for the samples totally reduced to magnetite, M_S results to increase with the dehydration temperature T_d, providing the maximum values for the sample S2-400-P.

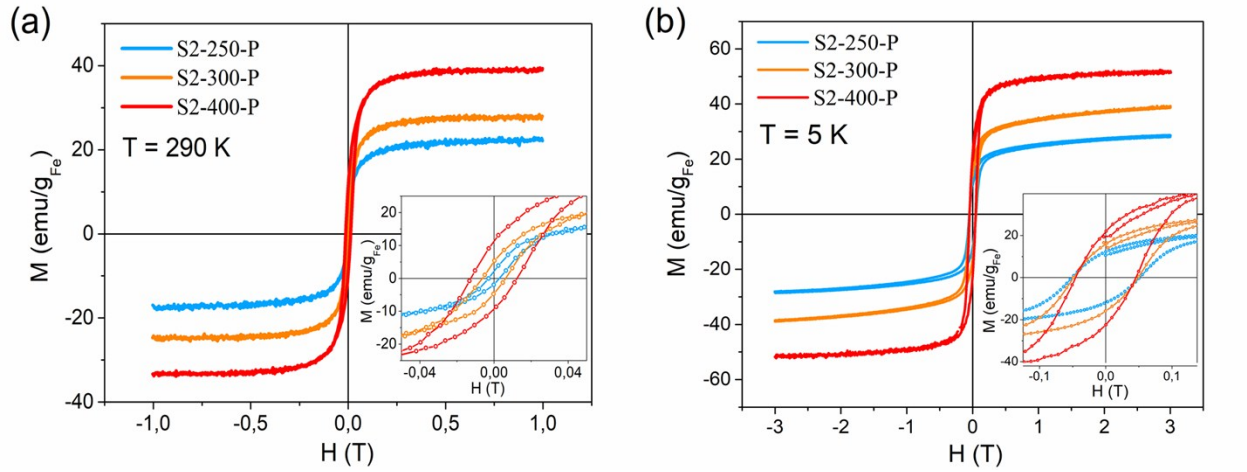

Figure S5. Hysteresis loop at T = 290 K (a) and a T = 5 K (b) for the three samples partially reduced to magnetite. In the insets a detail of the coercive field of the samples is shown. It can be observed that higher T_d leads to higher M_S and increasing H_C.

Table S6. - Saturation magnetization M_S and coercive field H_C of the partially reduced samples as evaluated from the VSM measurements.

Sample	M_S (290 K) (emu/g_{Fe})	H_C (290 K) (mT)	M_S (5 K) (emu/g_{Fe})	H_C (5 K) (mT)
S2-250-P	22.8 ± 1.1	2.93 ± 0.15	29.6 ± 1.5	51.1 ± 2.5
S2-300-P	27.7 ± 1.4	6.35 ± 0.31	42.6 ± 2.1	49.0 ± 2.5
S2-400-P	39.2 ± 2.0	12.4 ± 0.6	50.8 ± 2.5	45.6 ± 2.3

Comparing the saturation magnetization of the totally (Table 3) and partially (Table S6) reduced samples, a clear difference is observed, since M_S is lower in the case of the partially reduced samples. This result is in agreement with the antiferromagnetic nature of hematite.

Moreover, at room temperature the totally reduced samples have slightly lower values of H_C than those of the partially reduced ones, which could be due to the presence of dipolar interactions

between particles in the first case. For partially reduced particles, magnetic cores are dispersed in a non-magnetic matrix keeping them apart.

At low temperature the differences between the samples are no longer observed and a similar loop opening is recorded for all the totally and partially reduced samples.

NMR results

To distinguish magnetite and hematite contributions in the partially reduced samples, we measured the relaxometric properties of the three hematite precursors prepared with the strategy S2 at different T_d (Fig. S6), dispersed in water at a mean iron concentration of about 10 mM. Both the longitudinal and transversal relaxivities of the hematite samples resulted to be lower than 1 mM^{-1} s^{-1} at all the investigated Larmor frequencies. Such a low value is consistent with the antiferromagnetic nature of hematite, since water protons are only sensitive to the hyperfine field fluctuations arising from unbalanced sublattice electronic magnetization. Hematite contribution to the relaxivity of the partially reduced samples can therefore be considered negligible.

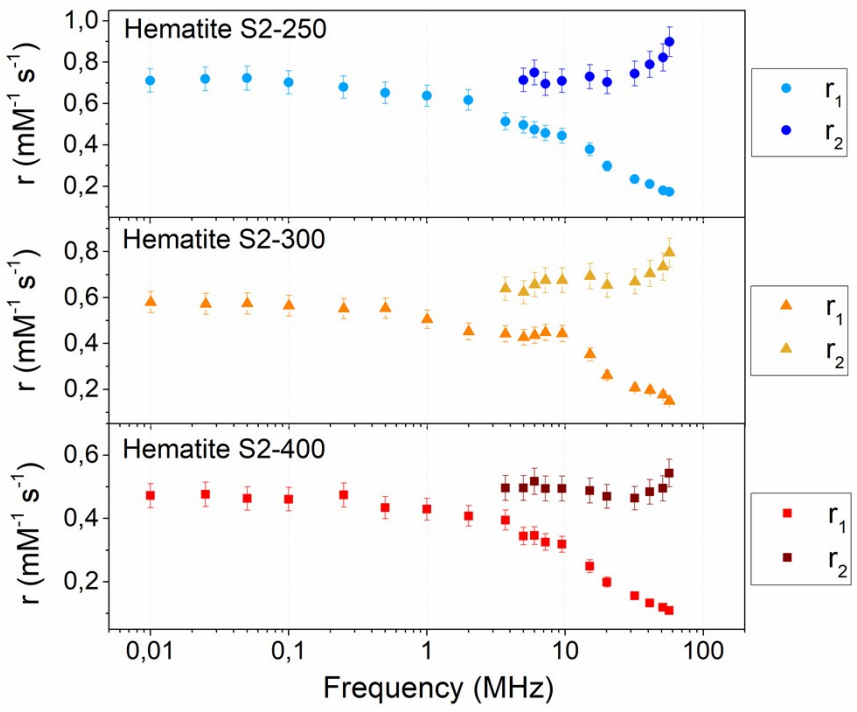

Figure S6. Longitudinal r_1 and transversal r_2 NMR-D profiles collected at room temperature in the Larmor frequency range $0.01 \leq \nu_L \leq 56.7$ MHz for the three hematite precursors. Relaxivity values are due to the magnetic nature of these samples, and decrease with the dehydration temperature T_d, being higher for the hematite sample S2-250 and lower for the sample S2-400.

Two more observation can be drawn from Fig. S6: (i) no signs of aggregations are observed, as expected for antiferromagnetic materials, since both r_1 and r_2 converge to the same value at low Larmor frequencies; (ii) the relaxivity values, although small, rescale with the dehydration temperature T_d, being higher for the hematite sample S2-250 and lower for the sample S2-400. For example, at ν_L= 56.7 MHz the r_2 values decrease from 0.90 mM^{-1} s^{-1} for the sample S2-250, to 0.80 mM^{-1} s^{-1} for the sample S2-300 and finally to 0.54 mM^{-1} s^{-1} for the sample S2-400.

In Fig. S7, the NMR-D profiles of the three samples partially reduced to magnetite are reported. It is worth nothing that the effects of a porous structure and a mixed composition of the magnetic core of the e-MNPs have been already studied by Rebolledo et al.[6] with e-MNPs made by a porous hematite matrix embedding nanosized clusters of magnetite, doped with Mn, Ni, Cu or Sn and surrounded with an alumina external layer. Samples described in ref. 6 showed outstanding values of transversal relaxivity ($r_2 \approx 402$ mM^{-1} s^{-1} for Mn doped e-MNPs) at 1.41 tesla (T) thanks to the increased dipolar field coming from the interactions among the iron oxide clusters and the decreased proton-cluster distance induced by the porosity (water penetrates within the pores). Contrary from samples described in ref. 6, the composition of our systems is strictly restricted to iron oxides, and the coating is also different. Therefore, a direct comparison between our compounds and the ones reported by Rebolledo et al.[6] could be misleading. Moreover, in our samples no particular advantages from a mixed composition of magnetite and hematite were found, being the performances of the partially reduced samples always lower than those of the totally reduced samples reported in Fig. 6.

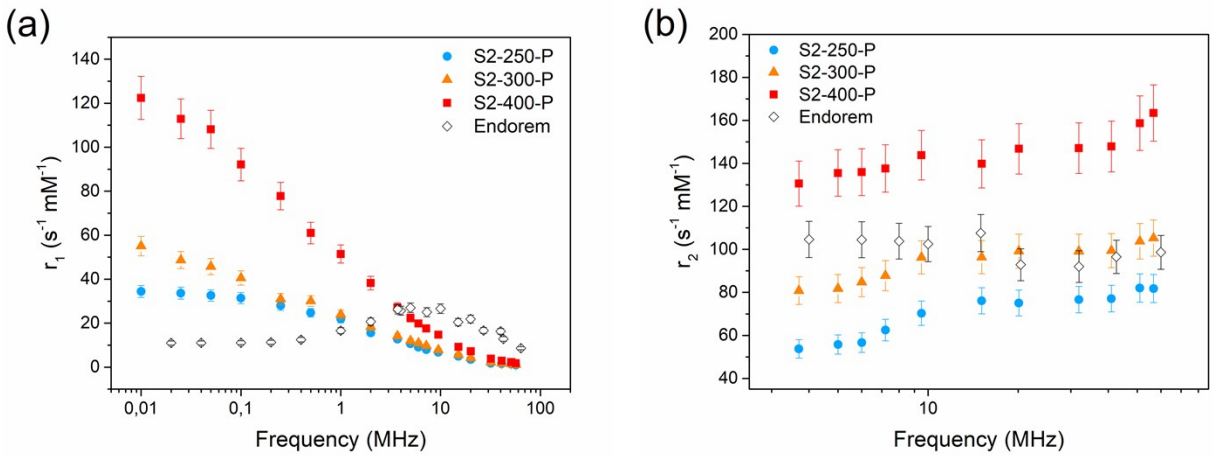

Figure S7. Longitudinal r_1 (a) and transversal r_2 (b) NMR-D profiles collected at room temperature in the Larmor frequency range $0.01 \leq \nu_L \leq 56.7$ MHz for the three samples partially reduced to magnetite. For comparison, the relaxivity values of Endorem as reported by Basini et al.[7] are shown. S2-400-P, the least porous sample, shows the highest r_1 and r_2 values, in good agreement with the differences observed in the magnetic characterization.

Both the trends of r_1 and r_2 vs ν_L shown in Fig.S7a and S7b and the scaling of the relaxivity values between the samples S2-250-P, S2-300-P and S2-400-P follow exactly the same behaviour of the

totally reduced samples, although one observes lower values of r_1 and r_2 due to the presence of the antiferromagnetic hematite. Comparing the curves in Fig. S7a with those in Fig. 6a, and the curves in Fig. S7b with those in Fig. 6b, only a decrease in the absolute values of r_1 and r_2 is observed, while the shape of the curves is preserved. This behaviour may be interpreted as a clear sign of the differences in the morphological properties of the three hematite precursors (S2-250, S2-300 and S2-400), here included the porosity. In fact, the partial or total reduction affects only the saturation magnetization of the samples, i.e. the amount of magnetite within the e-MNPs, and consequently the relaxivity values.

The rescaling of the r_2 values among the three partially reduced samples is even more clear than in the case of the totally reduced samples. At ν_L = 56.7 MHz r_2 decreases from 163 mM^{-1} s^{-1} for the sample S2-400-P to 105 mM^{-1} s^{-1} for the sample S2-300-P, and finally to 82 mM^{-1} s^{-1} for the sample S2-250-P. Moreover, r_2 values are roughly comparable to those of Endorem (Fig. S7b), being the sample S2-400-P the most efficient one.

MFH results

Fig. S8a and S8b show the SAR of the three partially reduced samples at f = 109 kHz and f = 202 kHz, respectively.

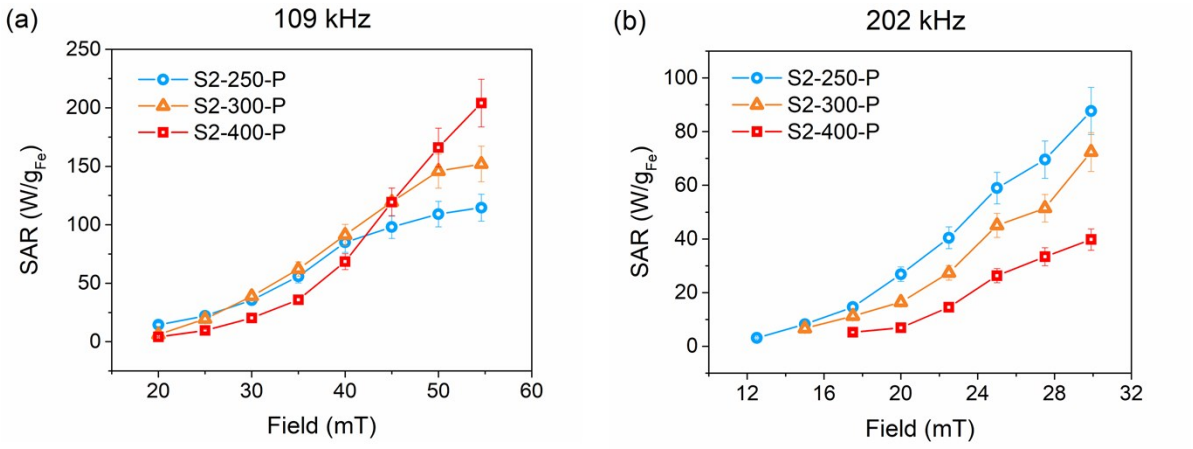

Figure S8. SAR as a function of the amplitude of the applied alternating magnetic field at f = 109 kHz (a) and f = 202 kHz (b) for the three samples partially reduced to magnetite. Sample S2-400-P, which corresponds to e-MNPs with least porosity, shows the highest SAR values at high field amplitudes.

As for the NMR results, the shape of the SAR(H) curves of the partially reduced samples are very similar to those of the totally reduced samples showed in Fig. 7, although translated to lower SAR values due to the minor volume of ferrimagnetic magnetite within the particles (the maximum SAR = 204 W/g is obtained for the sample S2-400-P at 109 kHz and 55 mT). Evidently, the presence of antiferromagnetic hematite in the partially reduced samples decreases their heating efficiency due to their lower M_S values. A superparamagnetic behaviour of small magnetite clusters embedded within the hematite matrix, if any, does not cause an increment of the e-MNPs heating

efficiency, being the SAR of the partially reduced samples similar to that of the totally reduced samples at low fields ($\sim 15-20$ mT) and much lower at high fields. The interest towards these samples was indeed justified by a possible superparamagnetic behaviour of small magnetite clusters embedded within a hematite matrix, that could increase the e-MNPs heating efficiency at the clinical fields of MFH. However, this occurrence was not verified.

References

1 M. Ohmori and E. MatijeviĆ, *J. Colloid Interface Sci.*, 1993, **160**(2), 288-292.

2 L. M. Liz-Marzán, M. Giersig and P. Mulvaney, *Langmuir*, 1995, **176**(2), 459-466.

3 R. M. Cornell and U. Schwertmann, The iron oxides: structure, properties, reactions, occurrences and uses, John Wiley & Sons, 2003.

4 H. Gavilán, O. Posth, L. K. Bogart, U. Steinhoff, L. Gutiérrez and M. P. Morales, *Acta Mater.*, 2017, **125**, 416-424.

5 Malvern Instruments. Zetasizer nano series user manual. MAN0317, **1**, 2004.

6 A. F. Rebolledo, S. Laurent, M. Calero, A. Villanueva, M. Knobel, J. F. Marco and P. Tartaj, *ACS Nano*, 2010, **4**(4), 2095-2103.

7 M. Basini, A. Guerrini, M. Cobianchi, F. Orsini, D. Bettega, M. Avolio, C. Innocenti, C. Sangregorio, A. Lascialfari and P. Arosio, *J. Alloys Compd.*, 2019, **770**, 58-66